

An average-derivative optimal scheme for frequency-domain scalar wave equation

Jing-Bo Chen¹

ABSTRACT

Forward modeling is an important foundation of full-waveform inversion. The rotated optimal nine-point scheme is an efficient algorithm for frequency-domain 2D scalar wave equation simulation, but this scheme fails when directional sampling intervals are different. To overcome the restriction on directional sampling intervals of the rotated optimal nine-point scheme, I introduce a new finite-difference algorithm. Based on an average-derivative technique, this new algorithm uses a nine-point operator to approximate spatial derivatives and mass acceleration term. The coefficients can be determined by minimizing phase-velocity dispersion errors. The resulting nine-point optimal scheme applies to equal and unequal directional sampling intervals, and can be regarded a generalization of the rotated optimal nine-point scheme. Compared to the classical five-point scheme, the number of grid points per smallest wavelength is reduced from 13 to less than four by this new nine-point optimal scheme for equal and unequal directional sampling intervals. Three numerical examples are presented to demonstrate the theoretical analysis. The average-derivative algorithm is also extended to a 2D viscous scalar wave equation and a 3D scalar wave equation.

INTRODUCTION

Full-waveform inversion (FWI) is a full-wavefield-modeling-based data-fitting process to extract structural information of subsurface from seismograms (Virieux and Operto, 2009). FWI can be classified into two categories: time-domain FWI (Tarantola, 1984; Gauthier et al., 1986; Boonyasirawat et al., 2009) and frequency-domain FWI (Pratt and Worthington, 1990; Pratt et al., 1998; Pratt, 1999).

An important part of FWI is forward modeling. Compared with time-domain modeling (Chen, 2009, 2011), frequency-domain modeling has its advantages: convenient manipulations of a single frequency, multishot computation based on a direct solver, and easy implementation of attenuation (Jo et al., 1996). Another advantage of frequency-domain modeling is that no wavefield-storage issue occurs when constructing the gradient of FWI in comparison with the time-domain modeling (Symes, 2007; Clapp, 2009). The main disadvantage of frequency-domain modeling is that it only can be done implicitly by solving a set of linear equations. Compared to the time-domain modeling, this disadvantage is particularly challenging when it comes to 3D computation. Therefore, reducing the number of grid points per wavelength is in great demand in particular when Gaussian elimination techniques are used.

Based on a rotated coordinate system, Jo et al. (1996) developed a nine-point operator to approximate the Laplacian and the mass acceleration terms. The coefficients are determined by obtaining the best normalized phase-velocity dispersion curves. This nine-point scheme reduces the number of grid points per wavelength to less than four, and leads to significant reductions of computer memory and CPU time. Hustedt et al. (2004) and Operto et al. (2007) generalized the rotated-coordinate method to variable density case and 3D case, respectively. Min et al. (2000) developed a 25-point optimal scheme for frequency-domain elastic modeling which does not need rotated coordinate system, but their dispersion analysis was carried out only for equal directional sampling intervals.

A disadvantage of the rotated-coordinate method is that equal directional sampling intervals are required, and in practice directional sampling intervals usually are different. To overcome the disadvantage of the rotated optimal nine-point scheme, a new finite-difference scheme is introduced in this paper. This new scheme is based on an average-derivative approach (Chen, 2001, 2008) and imposes no restriction of equal directional sampling intervals. The coefficients can be determined by minimizing phase-velocity dispersion errors. The resulting average-derivative nine-point

Manuscript received by the Editor 4 October 2011; revised manuscript received 26 June 2012; published online 17 September 2012.

¹Chinese Academy of Sciences, Institute of Geology and Geophysics, Key Laboratory of Petroleum Resources Research, Beijing, China. E-mail: chenjb@mail.iggcas.ac.cn.

© 2012 Society of Exploration Geophysicists. All rights reserved.

scheme reduces the number of grid points per wavelength to less than four for equal and unequal directional sampling intervals.

In the next section, I will present the rotated optimal nine-point scheme and point out its limitations. This is followed by the introduction of an average-derivative optimal nine-point scheme, the optimization of coefficients, and a numerical dispersion analysis. Numerical examples are then presented to demonstrate the theoretical analysis. Finally, I will generalize the average-derivative method to the viscous scalar wave equation and 3D wave equation.

CLASSICAL NINE-POINT SCHEME AND ITS LIMITATIONS

Consider the 2D scalar wave equation in the frequency domain

$$\frac{\partial^2 P}{\partial x^2} + \frac{\partial^2 P}{\partial z^2} + \frac{\omega^2}{v^2} P = 0, \tag{1}$$

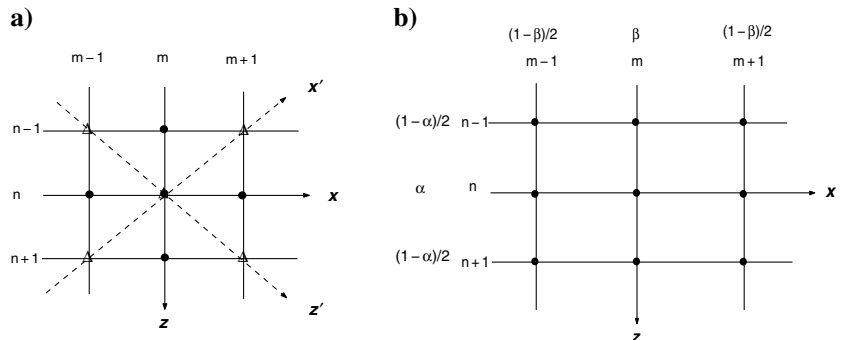
where P is the pressure wavefield, ω is circular frequency, and $v(x, y)$ is the velocity. To compare with the result in Jo et al. (1996), I first consider the 2D case. Later, the 3D case will be discussed.

A nine-point scheme for equation 1 was introduced by Jo et al. (1996)

$$\begin{aligned} & a \frac{P_{m+1,n} + P_{m-1,n} - 4P_{m,n} + P_{m,n+1} + P_{m,n-1}}{\Delta^2} \\ & + (1-a) \frac{P_{m+1,n+1} + P_{m-1,n+1} - 4P_{m,n} + P_{m+1,n-1} + P_{m-1,n-1}}{2\Delta^2} \\ & + \frac{\omega^2}{v_{m,n}^2} (cP_{m,n} + d(P_{m+1,n} + P_{m-1,n} + P_{m,n+1} + P_{m,n-1})) \\ & + e(P_{m+1,n+1} + P_{m-1,n+1} + P_{m+1,n-1} + P_{m-1,n-1}) = 0, \end{aligned} \tag{2}$$

where $P_{m,n} \approx P(m\Delta x, n\Delta z)$, $v_{m,n} \approx v(m\Delta x, n\Delta z)$, and Δx and Δz are directional sampling intervals in the x -direction and z -direction, respectively. Here $\Delta x = \Delta z = \Delta$. The constants a , c , and d are weighted coefficients, and $e = \frac{1-c-4d}{4}$. For details, see Figure 1a.

Figure 1. Schematic of the rotated optimal nine-point scheme (a), and the average-derivative optimal nine-point scheme (b).



Note that a variant of scheme 2 can be obtained

$$\begin{aligned} & a \frac{P_{m+1,n} + P_{m-1,n} - 4P_{m,n} + P_{m,n+1} + P_{m,n-1}}{\Delta^2} \\ & + (1-a) \frac{P_{m+1,n+1} + P_{m-1,n+1} - 4P_{m,n} + P_{m+1,n-1} + P_{m-1,n-1}}{2\Delta^2} \\ & + \omega^2 \left[c \frac{P_{m,n}}{v_{m,n}^2} + d \left(\frac{P_{m+1,n}}{v_{m+1,n}^2} + \frac{P_{m-1,n}}{v_{m-1,n}^2} + \frac{P_{m,n+1}}{v_{m,n+1}^2} + \frac{P_{m,n-1}}{v_{m,n-1}^2} \right) \right. \\ & \left. + e \left(\frac{P_{m+1,n+1}}{v_{m+1,n+1}^2} + \frac{P_{m-1,n+1}}{v_{m-1,n+1}^2} + \frac{P_{m+1,n-1}}{v_{m+1,n-1}^2} + \frac{P_{m-1,n-1}}{v_{m-1,n-1}^2} \right) \right] = 0. \end{aligned} \tag{3}$$

According to numerical experiments, schemes 2 and 3 have very similar performance.

The rotated nine-point optimal scheme 2 with coefficients ($a = 0.5461$, $c = 0.6248$, and $d = 0.0938$) reduces the number of grid points per shortest wavelength to less than four, and results in remarkable reductions of computer storage and CPU time. However, this scheme has a requirement of $\Delta x = \Delta z$, which is not always fulfilled. For example, the horizontal and vertical sampling intervals of the Marmousi model are $dx = 12.5$ m and $dz = 4$ m, respectively. For such a model, the rotated nine-point optimal scheme 2 fails. Now I try to develop a generalization of scheme 2. The generalization is required to be also valid for $\Delta x \neq \Delta z$. A natural guess for this generalization is

$$\begin{aligned} & a \left[\frac{P_{m+1,n} - 2P_{m,n} + P_{m-1,n}}{\Delta x^2} + \frac{P_{m,n+1} - 2P_{m,n} + P_{m,n-1}}{\Delta z^2} \right] \\ & + (1-a) \frac{P_{m+1,n+1} + P_{m-1,n+1} - 4P_{m,n} + P_{m+1,n-1} + P_{m-1,n-1}}{\Delta x^2 + \Delta z^2} \\ & + \frac{\omega^2}{v_{m,n}^2} (cP_{m,n} + d(P_{m+1,n} + P_{m-1,n} + P_{m,n+1} + P_{m,n-1})) \\ & + e(P_{m+1,n+1} + P_{m-1,n+1} + P_{m+1,n-1} + P_{m-1,n-1}) = 0. \end{aligned} \tag{4}$$

Unfortunately, however, scheme 4 is wrong because the second term on the left side of scheme 4 is not an approximation of the Laplacian when $\Delta x \neq \Delta z$.

In fact, using Taylor expansion, one can obtain

$$\begin{aligned} & \frac{P_{m+1,n+1} + P_{m-1,n+1} - 4P_{m,n} + P_{m+1,n-1} + P_{m-1,n-1}}{\Delta x^2 + \Delta z^2} \\ & = \frac{2\Delta x^2}{\Delta x^2 + \Delta z^2} \frac{\partial^2 P}{\partial x^2}(m, n) + \frac{2\Delta z^2}{\Delta x^2 + \Delta z^2} \frac{\partial^2 P}{\partial z^2}(m, n) \\ & + \mathcal{O}((\Delta x, \Delta z)^2). \end{aligned} \tag{5}$$

When $\Delta x \neq \Delta z$, the left side of equation 5 is not an approximation of the Laplacian $\frac{\partial^2 P}{\partial x^2} + \frac{\partial^2 P}{\partial z^2}$ at point (m, n) because $\frac{2\Delta x^2}{\Delta x^2 + \Delta z^2} \neq \frac{2\Delta z^2}{\Delta x^2 + \Delta z^2}$.

Therefore, another approach should be developed to achieve a generalization of scheme 2 to the case which also allows $\Delta x \neq \Delta z$.

An average-derivative scheme

Based on an average-derivative technique (Chen, 2001, 2008), I introduce an average-derivative scheme for equation 1

$$\begin{aligned} & \frac{\bar{P}_{m+1,n} - 2\bar{P}_{m,n} + \bar{P}_{m-1,n}}{\Delta x^2} + \frac{\tilde{P}_{m,n+1} - 2\tilde{P}_{m,n} + \tilde{P}_{m,n-1}}{\Delta z^2} \\ & + \frac{\omega^2}{v_{m,n}^2} (cP_{m,n} + d(P_{m+1,n} + P_{m-1,n} + P_{m,n+1} + P_{m,n-1}) \\ & + e(P_{m+1,n+1} + P_{m-1,n+1} + P_{m+1,n-1} + P_{m-1,n-1})) = 0, \end{aligned} \tag{6}$$

where

$$\begin{aligned} \bar{P}_{m+1,n} &= \frac{1-\alpha}{2} P_{m+1,n+1} + \alpha P_{m+1,n} + \frac{1-\alpha}{2} P_{m+1,n-1}, \\ \bar{P}_{m,n} &= \frac{1-\alpha}{2} P_{m,n+1} + \alpha P_{m,n} + \frac{1-\alpha}{2} P_{m,n-1}, \\ \bar{P}_{m-1,n} &= \frac{1-\alpha}{2} P_{m-1,n+1} + \alpha P_{m-1,n} + \frac{1-\alpha}{2} P_{m-1,n-1}, \end{aligned} \tag{7}$$

and

$$\begin{aligned} \tilde{P}_{m,n+1} &= \frac{1-\beta}{2} P_{m+1,n+1} + \beta P_{m,n+1} + \frac{1-\beta}{2} P_{m-1,n+1}, \\ \tilde{P}_{m,n} &= \frac{1-\beta}{2} P_{m+1,n} + \beta P_{m,n} + \frac{1-\beta}{2} P_{m-1,n}, \\ \tilde{P}_{m,n-1} &= \frac{1-\beta}{2} P_{m+1,n-1} + \beta P_{m,n-1} + \frac{1-\beta}{2} P_{m-1,n-1}, \end{aligned} \tag{8}$$

where α, β, c , and d are weighted coefficients and $e = \frac{1-c-4d}{4}$. For details, see Figure 1b.

In equation 6, the approximations of the derivatives are weighted averages of three approximations, and therefore, I call the equation 6 the average-derivative nine-point scheme. The motivation of the average-derivative method is to provide a family of approximations to the derivatives from which the optimization approximation can be chosen to meet our need. Scheme 6 applies to $\Delta x = \Delta z$ and $\Delta x \neq \Delta z$ as well. Furthermore, the average-derivative nine-point scheme 6 includes the rotated nine-point scheme 2 as a special case because when $\Delta x = \Delta z = \Delta$, and $\alpha = \beta$, scheme 6 becomes

$$\begin{aligned} & \tilde{\alpha} \frac{P_{m+1,n} + P_{m-1,n} - 4P_{m,n} + P_{m,n+1} + P_{m,n-1}}{\Delta^2} \\ & + (1 - \tilde{\alpha}) \frac{P_{m+1,n+1} + P_{m-1,n+1} - 4P_{m,n} + P_{m+1,n-1} + P_{m-1,n-1}}{2\Delta^2} \\ & + \frac{\omega^2}{v_{m,n}^2} (cP_{m,n} + d(P_{m+1,n} + P_{m-1,n} + P_{m,n+1} + P_{m,n-1}) \\ & + e(P_{m+1,n+1} + P_{m-1,n+1} + P_{m+1,n-1} + P_{m-1,n-1})) = 0, \end{aligned} \tag{9}$$

where $\tilde{\alpha} = 2\alpha - 1$.

Therefore, the average-derivative nine-point scheme 6 is just the scheme which achieves the generalization of scheme 2 to the situation where $\Delta x = \Delta z$ and $\Delta x \neq \Delta z$ are allowed. This new scheme increases the flexibility of scheme 2, and one can directly deals with a velocity model without the requirement of $\Delta x = \Delta z$.

In addition, the average-derivative nine-point scheme 6 also includes the classical five-point scheme as a special case because when $\alpha = 1, \beta = 1, c = 1$, and $d = 0$, scheme 6 becomes

$$\begin{aligned} & \frac{P_{m+1,n} - 2P_{m,n} + P_{m-1,n}}{\Delta x^2} + \frac{P_{m,n+1} - 2P_{m,n} + P_{m,n-1}}{\Delta z^2} \\ & + \frac{\omega^2}{v_{m,n}^2} P_{m,n} = 0. \end{aligned} \tag{10}$$

OPTIMIZATION AND DISPERSION ANALYSIS

In this Section, I perform optimization of the coefficients and show that the average-derivative nine-point scheme 6 retains the advantages of the rotated nine-point scheme 2.

Substituting $P(x, z, \omega) = P_0 e^{-i(k_x x + k_z z)}$ into equation 6 and assuming a constant v , one obtains the discrete dispersion relation

$$\frac{\omega^2}{v^2} = \frac{[(1-\alpha)\cos(k_z \Delta z) + \alpha](2-2\cos(k_x \Delta x)) + r^2[(1-\beta)\cos(k_x \Delta x) + \beta](2-2\cos(k_z \Delta z))}{\Delta x^2 [c + 2d(\cos(k_z \Delta z) + \cos(k_x \Delta x)) + 4e \cos(k_x \Delta x) \cos(k_z \Delta z)]} \tag{11}$$

where $r = \frac{\Delta x}{\Delta z}$. Here, I first consider the case $\Delta x \geq \Delta z$.

From equation 11, the normalized phase velocity can be derived as follows

$$\frac{v_{ph}}{v} = \frac{\left\{ [(1-\alpha)\cos\left(\frac{2\pi \cos \theta}{rG}\right) + \alpha] \sin^2\left(\frac{\pi \sin \theta}{G}\right) + r^2 \left[(1-\beta)\cos\left(\frac{2\pi \sin \theta}{G}\right) + \beta \right] \sin^2\left(\frac{\pi \cos \theta}{rG}\right) \right\}^{\frac{1}{2}}}{\frac{\pi}{G} \left\{ c + 2d \left[\cos\left(\frac{2\pi \cos \theta}{rG}\right) + \cos\left(\frac{2\pi \sin \theta}{G}\right) \right] + 4e \cos\left(\frac{2\pi \cos \theta}{rG}\right) \cos\left(\frac{2\pi \sin \theta}{G}\right) \right\}^{\frac{1}{2}}} \tag{12}$$

Table 1. Optimization coefficients for α, β, c , and d for different $\frac{\Delta x}{\Delta z}$ when $\Delta x \geq \Delta z$.

	α	β	c	d
$\frac{\Delta x}{\Delta z} = 1$	0.79439418	0.79439295	0.63482698	0.09129325
$\frac{\Delta x}{\Delta z} = 1.5$	0.65838767	0.86350605	0.63737738	0.09065565
$\frac{\Delta x}{\Delta z} = 2$	0.47368041	0.88433462	0.63610225	0.09097443
$\frac{\Delta x}{\Delta z} = 2.5$	0.93518516	0.78323578	0.63575594	0.09106101
$\frac{\Delta x}{\Delta z} = 3$	0.87450770	0.79811153	0.63571545	0.09107113
$\frac{\Delta x}{\Delta z} = 3.5$	0.88428729	0.80056069	0.63575353	0.09106161
$\frac{\Delta x}{\Delta z} = 4$	0.86562975	0.80408611	0.63580498	0.09104875

where V_{ph} is the phase velocity and $k_x = k \sin \theta$, $k_z = k \cos \theta$, and $G = \frac{2\pi}{k\Delta x}$. When $\Delta x \neq \Delta z$, the quantity G is defined with respect to the larger sampling interval. That is why I separate the analysis for $\Delta x \geq \Delta z$ and $\Delta z > \Delta x$.

The coefficients α , β , c , and d are determined by minimizing the phase error

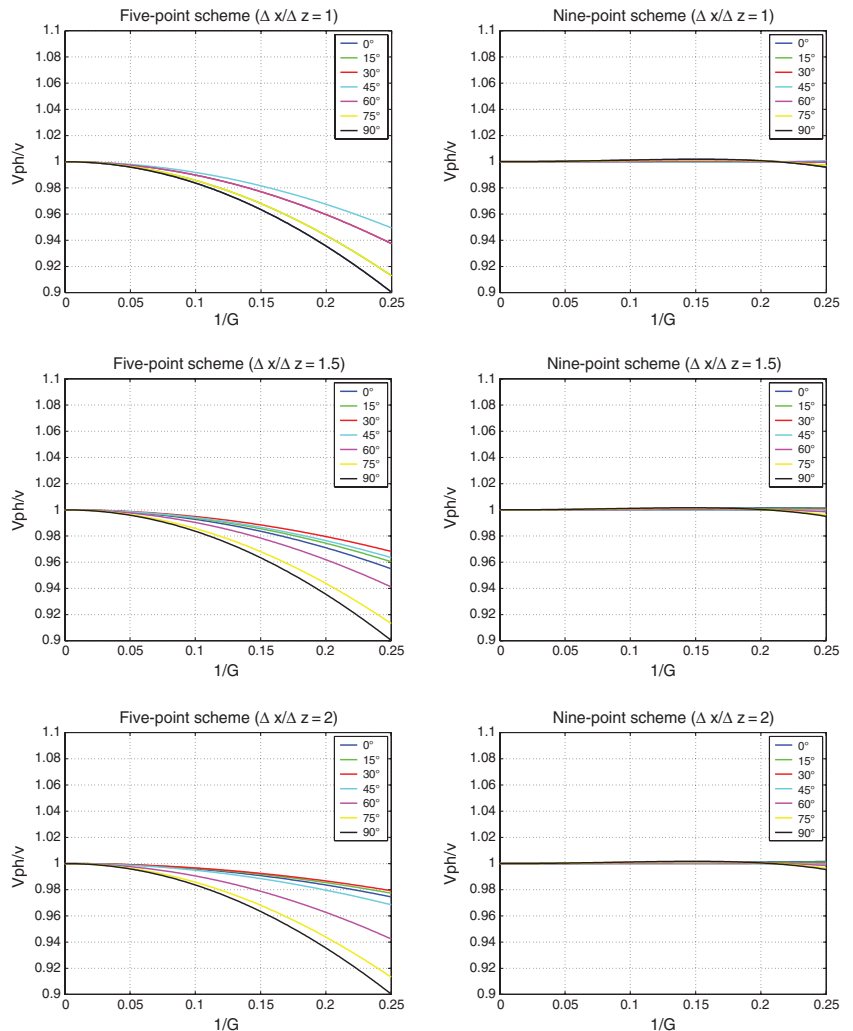
$$E(\alpha, \beta, c, d) = \iint \left[1 - \frac{V_{ph}(\theta, \tilde{k}; \alpha, \beta, c, d)}{v} \right]^2 d\tilde{k}d\theta, \quad (13)$$

where $\tilde{k} = \frac{1}{G}$.

Table 2. Optimization coefficients for α , β , c , and d for different $\frac{\Delta z}{\Delta x}$ when $\Delta x < \Delta z$.

	α	β	c	d
$\frac{\Delta z}{\Delta x} = 1.5$	0.86350605	0.65838767	0.63737738	0.09065565
$\frac{\Delta z}{\Delta x} = 2$	0.88433462	0.47368041	0.63610225	0.09097443
$\frac{\Delta z}{\Delta x} = 2.5$	0.78323578	0.93518516	0.63575594	0.09106101
$\frac{\Delta z}{\Delta x} = 3$	0.79811153	0.87450770	0.63571545	0.09107113
$\frac{\Delta z}{\Delta x} = 3.5$	0.80056069	0.88428729	0.63575353	0.09106161
$\frac{\Delta z}{\Delta x} = 4$	0.80408611	0.86562975	0.63580498	0.09104875

Figure 2. Normalized phase velocity curves of the five-point scheme 10 and the average-derivative optimal nine-point scheme 6 for different $\frac{\Delta x}{\Delta z}$ when $\Delta x \geq \Delta z$.



The ranges of \tilde{k} and θ are taken as $[0, 0.25]$ and $[0, \frac{\pi}{2}]$, respectively. A constrained nonlinear optimization program `fmincon` in MATLAB is used to determine the optimization coefficients. The optimization coefficients for different $r = \frac{\Delta x}{\Delta z}$ are listed in Table 1. One can see that the coefficients α and β varies with $\frac{\Delta x}{\Delta z}$, and the changes in coefficients c and d are small.

If $\Delta z > \Delta x$, the discrete dispersion relation becomes

$$\frac{\omega^2}{v^2} = \frac{r^2[(1-\alpha)\cos(k_z\Delta z) + \alpha](2-2\cos(k_x\Delta x)) + [(1-\beta)\cos(k_x\Delta x) + \beta](2-2\cos(k_z\Delta z))}{\Delta z^2[c + 2d(\cos(k_z\Delta z) + \cos(k_x\Delta x)) + 4e\cos(k_z\Delta z)\cos(k_x\Delta x)]}, \quad (14)$$

where $r = \frac{\Delta z}{\Delta x}$.

From equation 14, the normalized phase velocity can be derived as follows

$$\frac{v_{ph}}{v} = \frac{\left\{ r^2 \left[(1-\alpha) \cos\left(\frac{2\pi \cos \theta}{G}\right) + \alpha \right] \sin^2\left(\frac{\pi \sin \theta}{rG}\right) + \left[(1-\beta) \cos\left(\frac{2\pi \sin \theta}{rG}\right) + \beta \right] \sin^2\left(\frac{\pi \cos \theta}{G}\right) \right\}^{\frac{1}{2}}}{\frac{\pi}{G} \left\{ c + 2d \left[\cos\left(\frac{2\pi \cos \theta}{G}\right) + \cos\left(\frac{2\pi \sin \theta}{rG}\right) \right] + 4e \cos\left(\frac{2\pi \cos \theta}{G}\right) \cos\left(\frac{2\pi \sin \theta}{rG}\right) \right\}^{\frac{1}{2}}}, \quad (15)$$

where $k_x = k \sin \theta$, $k_z = k \cos \theta$, and $G = \frac{2\pi}{k\Delta z}$.

The optimization coefficients for the case of $\Delta z > \Delta x$ are listed in Table 2. Compared to the case of $\Delta x \geq \Delta z$, the only change is that the coefficients α and β are exchanged.

Now I perform numerical dispersion analysis. Figures 2 and 3 show normalized phase velocity curves of the five-point scheme 10 and the average-derivative optimal nine-point scheme 6 for different $\frac{\Delta x}{\Delta z}$ when $\Delta x \geq \Delta z$. Within the phase error of $\pm 1\%$, the five-point scheme 10 requires 13 grid points per shortest wavelength, while the average-derivative optimal nine-point scheme 6 requires less than four points. Figure 4 shows normalized phase velocity curves of the average-derivative optimal nine-point scheme 6 for different $\frac{\Delta z}{\Delta x}$ when $\Delta x < \Delta z$. In this case, the same conclusion

can be drawn with respect to the number of grid points per shortest wavelength.

GENERALIZATION OF SCHEME 6

Due to its flexibility and simplicity, average-derivative method can be easily extended to the viscous scalar and 3D cases. In this section, I briefly present the resulting schemes. Detailed discussion of these schemes is beyond the scope of the present paper.

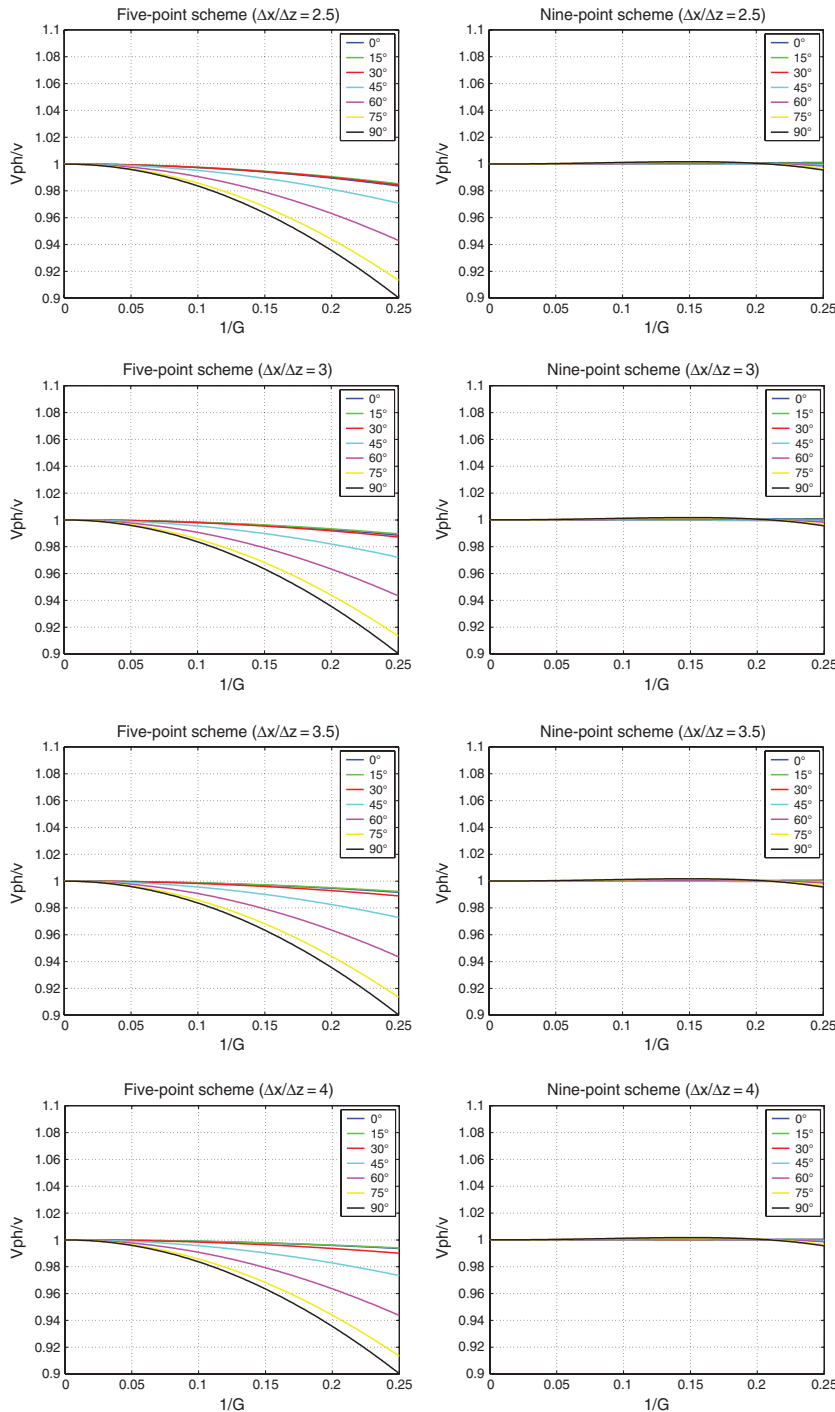


Figure 3. Normalized phase velocity curves of the five-point scheme 10 and the average-derivative optimal nine-point scheme 6 for different $\frac{\Delta x}{\Delta z}$ when $\Delta x \geq \Delta z$.

The viscous scalar case

The 2D viscous scalar wave equation reads

$$\frac{\partial}{\partial x} \left(\frac{1}{\rho} \frac{\partial P}{\partial x} \right) + \frac{\partial}{\partial z} \left(\frac{1}{\rho} \frac{\partial P}{\partial z} \right) + \frac{\omega^2}{\kappa} P = 0, \quad (16)$$

where $\rho(x, z)$ is the density, and $\kappa(x, z)$ is the complex bulk modulus which accounts for attenuation in one of the two ways

$$\kappa(x, z) = \rho(x, z) v^2(x, z) \left(1 - i \frac{1}{2Q} \right)^2, \quad (17)$$

$$\frac{1}{\kappa(x, z)} = \frac{1}{\rho(x, z)} \left(\frac{1}{v(x, z)} + \frac{1}{\pi v(x, z) Q} \text{Ln} \left| \frac{\omega_r}{\omega} \right| + i \frac{\text{sgn}(\omega)}{2v(x, z) Q} \right)^2, \quad (18)$$

where $v(x, t)$ is the real velocity, Q is the attenuation factor, i is the unit of imaginary numbers, sgn is the sign function, and ω_r is a reference frequency (Operto et al., 2007).

An average-derivative optimal nine-point scheme for equation 16 is

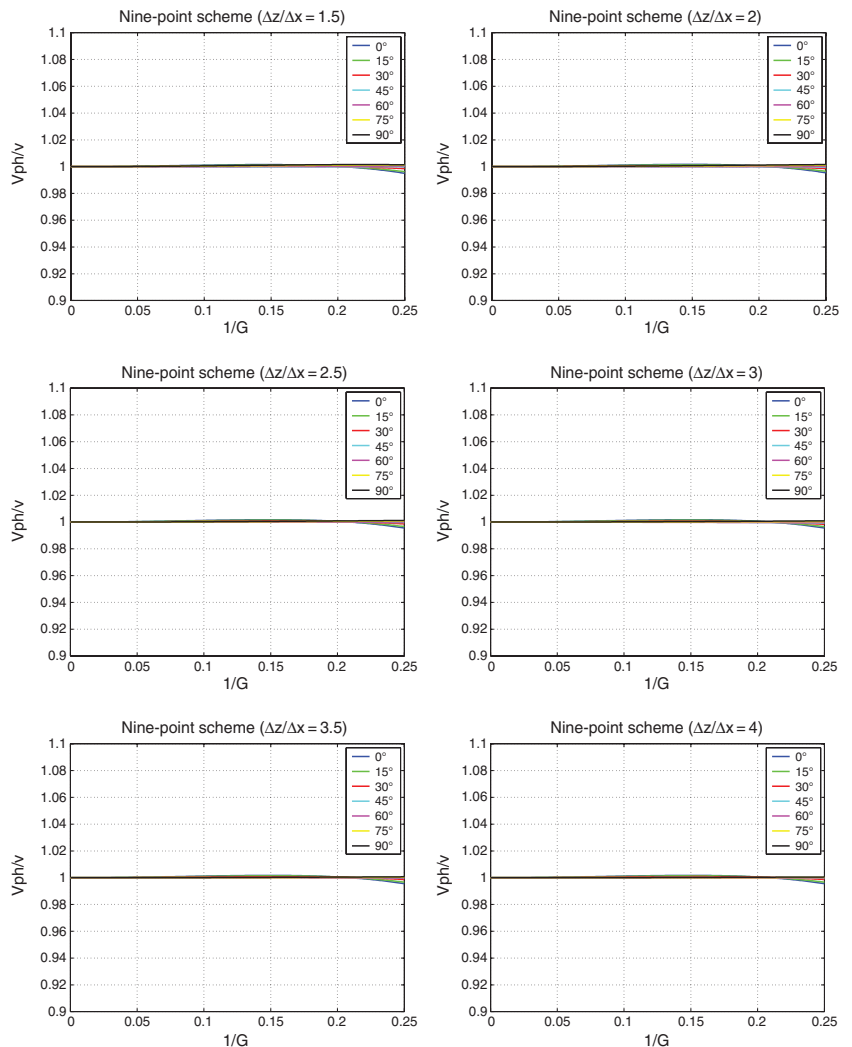
$$\begin{aligned} & \frac{1}{\Delta x^2} \left[\frac{1}{\rho_{m+\frac{1}{2},n}} \bar{P}_{m+1,n} - \left(\frac{1}{\rho_{m+\frac{1}{2},n}} + \frac{1}{\rho_{m-\frac{1}{2},n}} \right) \bar{P}_{m,n} + \frac{1}{\rho_{m-\frac{1}{2},n}} \bar{P}_{m-1,n} \right] \\ & + \frac{1}{\Delta z^2} \left[\frac{1}{\rho_{m,n+\frac{1}{2}}} \tilde{P}_{m,n+1} - \left(\frac{1}{\rho_{m,n+\frac{1}{2}}} + \frac{1}{\rho_{m,n-\frac{1}{2}}} \right) \tilde{P}_{m,n} + \frac{1}{\rho_{m,n-\frac{1}{2}}} \tilde{P}_{m,n-1} \right] \\ & + \frac{\omega^2}{\kappa_{m,n}^2} (cP_{m,n} + d(P_{m+1,n} + P_{m-1,n} + P_{m,n+1} + P_{m,n-1}) \\ & + e(P_{m+1,n+1} + P_{m-1,n+1} + P_{m+1,n-1} + P_{m-1,n-1})) = 0, \quad (19) \end{aligned}$$

where

$$\begin{aligned} \rho_{m+\frac{1}{2},n} &= \frac{1}{2}(\rho_{m,n} + \rho_{m+1,n}), \\ \rho_{m-\frac{1}{2},n} &= \frac{1}{2}(\rho_{m-1,n} + \rho_{m,n}), & \rho_{m,n+\frac{1}{2}} &= \frac{1}{2}(\rho_{m,n} + \rho_{m,n+1}), \\ \rho_{m,n-\frac{1}{2}} &= \frac{1}{2}(\rho_{m,n-1} + \rho_{m,n+1}), \end{aligned} \quad (20)$$

and

Figure 4. Normalized phase velocity curves of the average-derivative optimal nine-point scheme 6 for different $\frac{\Delta z}{\Delta x}$ when $\Delta x < \Delta z$.



$$\begin{aligned} \bar{P}_{m+1,n} &= \frac{1-\alpha}{2}P_{m+1,n+1} + \alpha P_{m+1,n} + \frac{1-\alpha}{2}P_{m+1,n-1}, \\ \bar{P}_{m,n} &= \frac{1-\alpha}{2}P_{m,n+1} + \alpha P_{m,n} + \frac{1-\alpha}{2}P_{m,n-1}, \\ \bar{P}_{m-1,n} &= \frac{1-\alpha}{2}P_{m-1,n+1} + \alpha P_{m-1,n} + \frac{1-\alpha}{2}P_{m-1,n-1}, \end{aligned} \quad (21)$$

and

$$\begin{aligned} \tilde{P}_{m,n+1} &= \frac{1-\beta}{2}P_{m+1,n+1} + \beta P_{m,n+1} + \frac{1-\beta}{2}P_{m-1,n+1}, \\ \tilde{P}_{m,n} &= \frac{1-\beta}{2}P_{m+1,n} + \beta P_{m,n} + \frac{1-\beta}{2}P_{m-1,n}, \\ \tilde{P}_{m,n-1} &= \frac{1-\beta}{2}P_{m+1,n-1} + \beta P_{m,n-1} + \frac{1-\beta}{2}P_{m-1,n-1}. \end{aligned} \quad (22)$$

Here, the coefficients $\alpha, \beta, c, d,$ and e are the same as in scheme 6.

The 3D case

Consider the 3D scalar wave equation

$$\frac{\partial^2 P}{\partial x^2} + \frac{\partial^2 P}{\partial y^2} + \frac{\partial^2 P}{\partial z^2} + \frac{\omega^2}{v^2}P = 0. \quad (23)$$

An average-derivative optimal 27-point scheme for equation 23 can be obtained as

$$\begin{aligned} &\frac{\bar{P}_{m+1,l,n} - 2\bar{P}_{m,l,n} + \bar{P}_{m-1,l,n}}{\Delta x^2} + \frac{\hat{P}_{m,l+1,n} - 2\hat{P}_{m,l,n} + \hat{P}_{m,l-1,n}}{\Delta y^2} \\ &+ \frac{\tilde{P}_{m,l,n+1} - 2\tilde{P}_{m,l,n} + \tilde{P}_{m,l,n-1}}{\Delta z^2} \\ &+ \frac{\omega^2}{v_{m,l,n}^2}(cP_{m,l,n} + dA + eB + fC) = 0, \end{aligned} \quad (24)$$

where $P_{m,l,n} \approx P(m\Delta x, l\Delta y, n\Delta z)$, $v_{m,l,n} \approx v(m\Delta x, l\Delta y, n\Delta z)$, and $\Delta x, \Delta y,$ and Δz are directional sampling intervals in the x -direction, y -direction, and z -direction, respectively, and

$$\begin{aligned} \bar{P}_{m+1,l,n} &= \alpha_1(P_{m+1,l+1,n} + P_{m+1,l,n+1} + P_{m+1,l-1,n} + P_{m+1,l,n-1}) \\ &+ \alpha_2(P_{m+1,l+1,n+1} + P_{m+1,l-1,n+1} + P_{m+1,l+1,n-1} + P_{m+1,l-1,n-1}) \\ &+ (1 - 4\alpha_1 - 4\alpha_2)P_{m+1,l,n} \\ \bar{P}_{m,l,n} &= \alpha_1(P_{m,l+1,n} + P_{m,l,n+1} + P_{m,l-1,n} + P_{m,l,n-1}) \\ &+ \alpha_2(P_{m,l+1,n+1} + P_{m,l-1,n+1} + P_{m,l+1,n-1} + P_{m,l-1,n-1}) \\ &+ (1 - 4\alpha_1 - 4\alpha_2)P_{m,l,n} \\ \bar{P}_{m-1,l,n} &= \alpha_1(P_{m-1,l+1,n} + P_{m-1,l,n+1} + P_{m-1,l-1,n} + P_{m-1,l,n-1}) \\ &+ \alpha_2(P_{m-1,l+1,n+1} + P_{m-1,l-1,n+1} + P_{m-1,l+1,n-1} + P_{m-1,l-1,n-1}) \\ &+ (1 - 4\alpha_1 - 4\alpha_2)P_{m-1,l,n}, \end{aligned} \quad (25)$$

$$\begin{aligned} \hat{P}_{m,l+1,n} &= \beta_1(P_{m+1,l+1,n} + P_{m,l+1,n+1} + P_{m-1,l+1,n} + P_{m,l+1,n-1}) \\ &+ \beta_2(P_{m+1,l+1,n+1} + P_{m+1,l+1,n-1} + P_{m-1,l+1,n+1} + P_{m-1,l+1,n-1}) \\ &+ (1 - 4\beta_1 - 4\beta_2)P_{m,l+1,n} \\ \hat{P}_{m,l,n} &= \beta_1(P_{m+1,l,n} + P_{m,l,n+1} + P_{m-1,l,n} + P_{m,l,n-1}) \\ &+ \beta_2(P_{m+1,l,n+1} + P_{m+1,l,n-1} + P_{m-1,l,n+1} + P_{m-1,l,n-1}) \\ &+ (1 - 4\beta_1 - 4\beta_2)P_{m,l,n} \\ \hat{P}_{m,l-1,n} &= \beta_1(P_{m+1,l-1,n} + P_{m,l-1,n+1} + P_{m-1,l-1,n} + P_{m,l-1,n-1}) \\ &+ \beta_2(P_{m+1,l-1,n+1} + P_{m+1,l-1,n-1} + P_{m-1,l-1,n+1} + P_{m-1,l-1,n-1}) \\ &+ (1 - 4\beta_1 - 4\beta_2)P_{m,l-1,n}, \end{aligned} \quad (26)$$

$$\begin{aligned} \tilde{P}_{m,l,n+1} &= \gamma_1(P_{m+1,l,n+1} + P_{m,l+1,n+1} + P_{m-1,l,n+1} + P_{m,l-1,n+1}) \\ &+ \gamma_2(P_{m+1,l+1,n+1} + P_{m+1,l-1,n+1} + P_{m-1,l+1,n+1} + P_{m-1,l-1,n+1}) \\ &+ (1 - 4\gamma_1 - 4\gamma_2)P_{m,l,n+1}, \\ \tilde{P}_{m,l,n} &= \gamma_1(P_{m+1,l,n} + P_{m,l+1,n} + P_{m-1,l,n} + P_{m,l-1,n}) \\ &+ \gamma_2(P_{m+1,l+1,n} + P_{m+1,l-1,n} + P_{m-1,l+1,n} + P_{m-1,l-1,n}) \\ &+ (1 - 4\gamma_1 - 4\gamma_2)P_{m,l,n}, \\ \tilde{P}_{m,l,n-1} &= \gamma_1(P_{m+1,l,n-1} + P_{m,l+1,n-1} + P_{m-1,l,n-1} + P_{m,l-1,n-1}) \\ &+ \gamma_2(P_{m+1,l+1,n-1} + P_{m+1,l-1,n-1} + P_{m-1,l+1,n-1} + P_{m-1,l-1,n-1}) \\ &+ (1 - 4\gamma_1 - 4\gamma_2)P_{m,l,n-1}, \end{aligned} \quad (27)$$

and

$$\begin{aligned} A &= (P_{m,l+1,n} + P_{m,l,n+1} + P_{m,l-1,n} + P_{m,l,n-1} + P_{m+1,l,n} + P_{m-1,l,n}) \\ B &= (P_{m+1,l+1,n} + P_{m+1,l,n+1} + P_{m+1,l-1,n} + P_{m+1,l,n-1} \\ &+ P_{m-1,l+1,n} + P_{m-1,l,n+1} \\ &+ P_{m-1,l-1,n} + P_{m-1,l,n-1} + P_{m,l+1,n+1} + P_{m,l-1,n+1} \\ &+ P_{m,l+1,n-1} + P_{m,l-1,n-1}) \\ C &= (P_{m+1,l+1,n+1} + P_{m+1,l-1,n+1} + P_{m+1,l+1,n-1} + P_{m+1,l-1,n-1} \\ &+ P_{m-1,l+1,n+1} + P_{m-1,l-1,n+1} + P_{m-1,l+1,n-1} + P_{m-1,l-1,n-1}). \end{aligned} \quad (28)$$

Here, $\alpha_1, \alpha_2, \beta_1, \beta_2, \gamma_1, \gamma_2, c, d,$ and e are coefficients which are to be optimized in the way as in the 2D case, and $f = \frac{1-c-6d-12e}{8}$.



Figure 5. Schematic of the homogeneous model.

NUMERICAL EXAMPLES

In this section, I present three numerical examples to verify the theoretical analysis on the average-derivative optimal nine-point scheme 6 and the classical five-point scheme 10.

First, I consider a homogeneous velocity model with a velocity of 3000 m/s (Figure 5). In this case, analytical solution is available to make comparisons with numerical solutions. Horizontal and vertical samplings are $n_x = 101$ and $n_z = 41$, respectively. A Ricker wavelet with peak frequency of 25 Hz is placed at the center of the model as a source, and a receiver is set 25 samples away from

the source horizontally. The maximum frequency used in the computation is 70 Hz. According to the criterion of four grid points per smallest wavelength, horizontal sampling interval is determined by $dx = 3000/75/4 \text{ m} \approx 11 \text{ m}$. Vertical sampling interval is taken as $dz = dx/1.5$. For this ratio of directional sampling intervals, the optimization coefficients of scheme 6 are $\alpha = 0.65838767$, $\beta = 0.65838767$, $c = 0.65838767$, and $d = 0.65838767$.

For the analytical solution, the following formula is used (Alford et al., 1974)

$$P(x, z, t) = i\pi\mathcal{F}^{-1} \left[H_0^{(2)} \left(\frac{\omega}{v} r \right) \mathcal{F}(f(t)) \right], \quad (29)$$

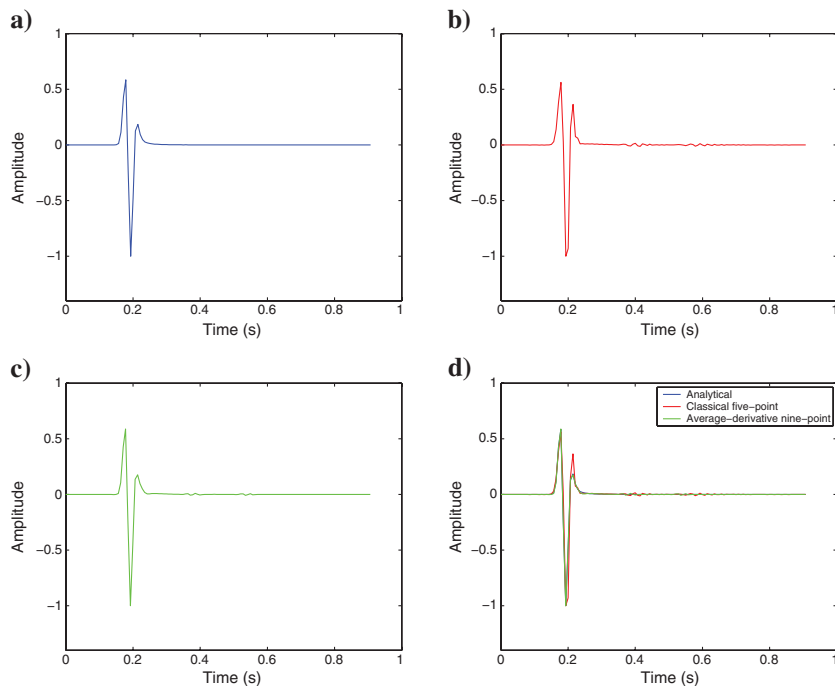


Figure 6. Seismograms computed with analytical method (a), classical five-point scheme (b), average-derivative optimal scheme (c) and the superimposed results (d).

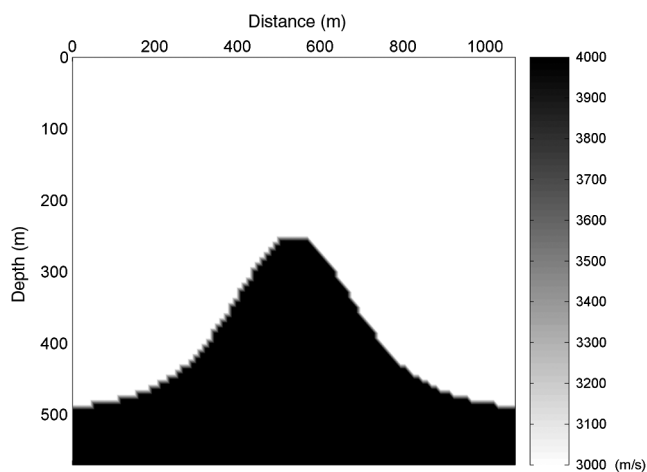


Figure 7. The salt dome velocity model.

where \mathcal{F} and \mathcal{F}^{-1} are Fourier and inverse Fourier transformations with respect to time, respectively, $f(t)$ is the Ricker wavelet, $H_0^{(2)}$ is the second Hankel function of order zero, and $r = \sqrt{(x - x_0)^2 + (z - z_0)^2}$. Here (x_0, z_0) is the source position.

Figure 6 shows the results computed with the analytical formula 29, the classical five-point scheme 10, and the average-derivative optimal scheme 6. The simulation result with the average-derivative optimal scheme 6 is in good agreement with the analytical result while the result with the classical five-point scheme 10 exhibits errors due to numerical dispersion.

Second, I consider a heterogeneous velocity model. Figure 7 shows a salt dome velocity model. The velocity of the salt dome is 4000 m/s, and the velocity of the overburden is 3000 m/s. Horizontal and vertical samplings are $n_x = 101$ and $n_z = 81$, respectively. A Ricker wavelet with peak frequency of 35 Hz is placed at the tenth level of the model as a source, and the receivers are set at the top of the model. The use of larger peak frequency in this example is to make the advantage of the average-derivative optimal scheme 6 more evident. Absorbing

boundary conditions with 45° one-way wave equation are used at the four sides of the model (Clayton and Engquist, 1977). The maximum frequency used in the computation, the horizontal and vertical sampling intervals, and the optimization coefficients are the same as those used in the homogeneous velocity model.

Figure 8 shows the seismograms computed with the classical five-point scheme 10, the average-derivative optimal scheme 6, and a fourth-order time-domain method presented in Alford et al. (1974). The simulation result with the classical five-point scheme 10 exhibits large numerical dispersion errors, particularly on the right side of the model. The result obtained with the average-derivative optimal nine-point scheme 6 has a much better performance in terms of numerical dispersion, and basically agree with the result with the fourth-order time-domain method.

Finally, I consider a more realistic model. Figure 9a shows part of the Marmousi model. The sampling intervals of the Marmousi model are $dx = 12.5 \text{ m}$ and $dz = 4 \text{ m}$. Horizontal and vertical samplings are $n_x = 301$ and $n_z = 301$, respectively. For this ratio of directional sampling intervals, the optimization coefficients

of scheme 6 are $\alpha = 0.87450770$, $\beta = 0.79811153$, $c = 0.63571545$, and $d = 0.09107113$. A Ricker wavelet with peak frequency of 12.5 Hz is placed at $(x = 625 \text{ m}, z = 36 \text{ m})$ as a source, and the receivers are set at the depth of 4 m with a spacing

of 12.5 m. Absorbing boundary conditions with 45° one-way wave equation are used at the four sides of the model.

Seismograms computed with the classical five-point scheme 10 and the average-derivative optimal scheme 6 are shown in Figure 9b

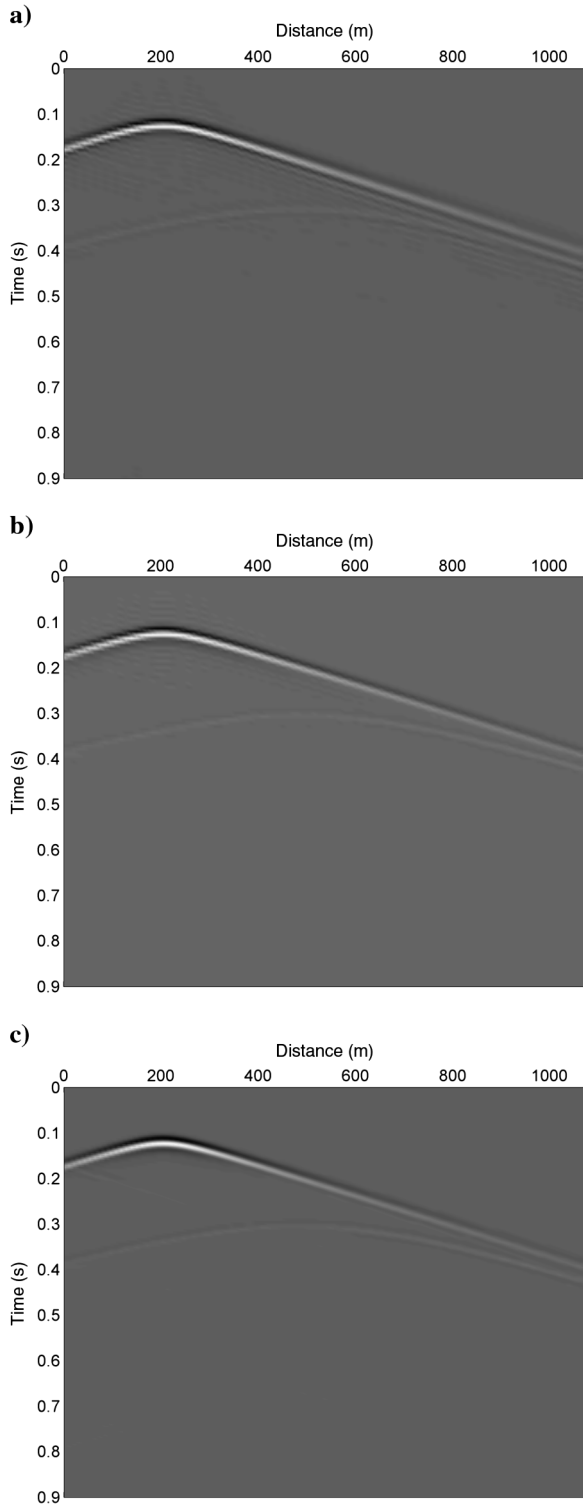


Figure 8. Seismograms computed with the classical five-point scheme (a), the average-derivative optimal scheme (b), and the time-domain fourth-order scheme (d).

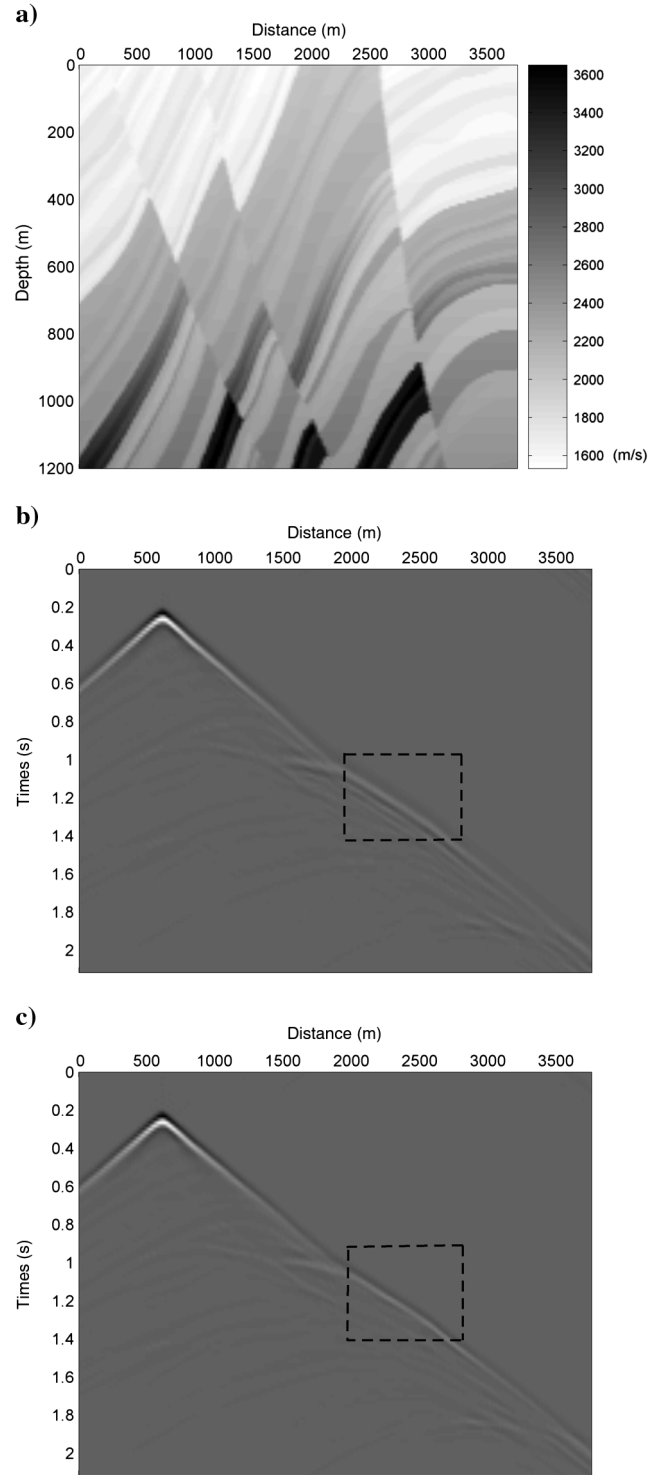


Figure 9. Part of the Marmousi model (a), and seismograms computed with the classical five-point scheme (b), the average-derivative optimal scheme (c).

and 9c, respectively. From the figures, one can see that the result of scheme 6 is better than that of scheme 10, particularly in the region highlighted by the dashed rectangles. For the Marmousi model, the traditional optimal nine-point scheme cannot be applied due to the fact of $dx \neq dz$, but the average-derivative optimal scheme still is valid due to its flexibility.

CONCLUSIONS

I have presented an average-derivative optimal nine-point scheme. This new scheme overcomes the disadvantage of the rotated optimal nine-point scheme by removing the requirement of equal directional sampling intervals. On the other hand, this new scheme retains the advantage of the rotated optimal nine-point scheme by reducing the number of grid points per shortest wavelength to less than four for equal and unequal directional sampling intervals. The average-derivative optimal nine-point scheme includes the rotated optimal nine-point scheme as a special case, and can be regarded as a generalization of the rotated optimal nine-point scheme to the case of general directional sampling intervals. Three numerical examples demonstrate the theoretical analysis.

ACKNOWLEDGMENTS

I would like to thank S. Operto, J. Cao, and anonymous reviewers for useful suggestions. This work is supported by the National Natural Science Foundation of China under grants 40830424, 40974074, and 40774069 and by the National Major Project of China (under grant 2011ZX05008-006).

REFERENCES

- Alford, R. M., K. R. Kelly, and D. M. Boore, 1974, Accuracy of finite-difference modeling of the acoustic wave equation: *Geophysics*, **39**, 834–842, doi: [10.1190/1.1440470](https://doi.org/10.1190/1.1440470).
- Boonyasiriwat, C., P. Valasek, P. Routh, W. Cao, G. T. Schuster, and B. Macy, 2009, An efficient multiscale method for time-domain waveform tomography: *Geophysics*, **74**, no. 6, WCC59–WCC68, doi: [10.1190/1.3151869](https://doi.org/10.1190/1.3151869).
- Chen, J.-B., 2001, New schemes for the nonlinear Schrödinger equation: *Applied Mathematics and Computation*, **124**, 371–379, doi: [10.1016/S0096-3003\(00\)00111-9](https://doi.org/10.1016/S0096-3003(00)00111-9).
- Chen, J.-B., 2008, Variational integrators and the finite element method: *Applied Mathematics and Computation*, **196**, 941–958, doi: [10.1016/j.amc.2007.07.028](https://doi.org/10.1016/j.amc.2007.07.028).
- Chen, J.-B., 2009, Lax-Wendroff and Nyström methods for seismic modeling: *Geophysical Prospecting*, **57**, 931–941, doi: [10.1111/gpr.2009.57.issue-6](https://doi.org/10.1111/gpr.2009.57.issue-6).
- Chen, J.-B., 2011, A stability formula for Lax-Wendroff methods with fourth-order in time and general-order in space for the scalar wave equation: *Geophysics*, **76**, no. 2, T37–T42, doi: [10.1190/1.3554626](https://doi.org/10.1190/1.3554626).
- Clapp, R. G., 2009, Reverse time migration with random boundaries: 79th Annual International Meeting, SEG, Expanded Abstracts, 2809–2813.
- Clayton, R., and B. Engquist, 1977, Absorbing boundary conditions for scalar and elastic wave equations: *Bulletin of the Seismological Society of America*, **67**, 1529–1540.
- Gauthier, O., J. Virieux, and A. Tarantola, 1986, Two-dimensional nonlinear inversion of seismic waveforms: *Geophysics*, **51**, 1387–1403, doi: [10.1190/1.1442188](https://doi.org/10.1190/1.1442188).
- Hustedt, B., S. Operto, and J. Virieux, 2004, Mixed-grid and staggered-grid finite-difference methods for frequency-domain acoustic wave modelling: *Geophysical Journal International*, **157**, 1269–1296, doi: [10.1111/j.1365-246X.2004.02289.x](https://doi.org/10.1111/j.1365-246X.2004.02289.x).
- Jo, C.-H., C. Shin, and J. H. Suh, 1996, An optimal 9-point, finite-difference, frequency-space, 2-D scalar wave extrapolator: *Geophysics*, **61**, 529–537, doi: [10.1190/1.1443979](https://doi.org/10.1190/1.1443979).
- Min, D.-J., C. Shin, B.-D. Kwon, and S. Chung, 2000, Improved frequency-domain elastic wave modeling using weighted-averaging difference operators: *Geophysics*, **65**, 884–895, doi: [10.1190/1.1444785](https://doi.org/10.1190/1.1444785).
- Operto, S., J. Virieux, P. Amestoy, J.-Y. L'Excellent, L. Giraud, and H. B. H. Ali, 2007, 3D finite-difference frequency-domain modeling of visco-acoustic wave propagation using a massively parallel direct solver: A feasibility study: *Geophysics*, **72**, no. 5, SM195–SM211, doi: [10.1190/1.2759835](https://doi.org/10.1190/1.2759835).
- Operto, S., J. Virieux, and F. Sourbier, 2007, Documentation of FWT2D program (version 4.8): Frequency-domain full-waveform modeling/inversion of wide-aperture seismic data for imaging 2D scalar media: Technical report N°007-SEISCOPE project.
- Pratt, R. G., 1999, Seismic waveform inversion in the frequency domain, Part I: Theory and verification in a physical scale model: *Geophysics*, **64**, 888–901, doi: [10.1190/1.1444597](https://doi.org/10.1190/1.1444597).
- Pratt, R. G., C. Shin, and G. J. Hicks, 1998, Gauss-Newton and full Newton methods in frequency-space seismic waveform inversion: *Geophysical Journal International*, **133**, 341–362, doi: [10.1046/j.1365-246X.1998.00498.x](https://doi.org/10.1046/j.1365-246X.1998.00498.x).
- Pratt, R. G., and M.-H. Worthington, 1990, Inverse theory applied to multi-source cross-hole tomography, Part I: Acoustic wave-equation method: *Geophysical Prospecting*, **38**, 287–310, doi: [10.1111/j.1365-2478.1990.tb01846.x](https://doi.org/10.1111/j.1365-2478.1990.tb01846.x).
- Symes, W. M., 2007, Reverse time migration with optimal checkpointing: *Geophysics*, **72**, no. 5, SM213–SM221, doi: [10.1190/1.2742686](https://doi.org/10.1190/1.2742686).
- Tarantola, A., 1984, Inversion of seismic reflection data in the acoustic approximation: *Geophysics*, **49**, 1259–1266, doi: [10.1190/1.1441754](https://doi.org/10.1190/1.1441754).
- Virieux, J., and S. Operto, 2009, An overview of full-waveform inversion in exploration geophysics: *Geophysics*, **74**, no. 6, WCC1–WCC26, doi: [10.1190/1.3238367](https://doi.org/10.1190/1.3238367).